Article

Voltage Control of Multiphase Cage Induction Generators at a Speed Varying over a Wide Range

Piotr Drozdowski (ID) **and Dariusz Cholewa ***

Faculty of Electrical and Computer Engineering, Cracow University of Technology, Warszawska 24 Str., 31-155 Cracow, Poland; pdrozdow@pk.edu.pl
* Correspondence: dariusz.cholewa@pk.edu.pl

Abstract: The subject of this publication is a method of controlling the DC voltage of a PWM rectifier supplied by a multiphase cage induction generator with the number of stator phases greater than three operating in a wide range of driving speeds. Voltage regulation is performed by changing the frequency and amplitude of the stator voltages with simultaneous switching of the phase sequence of these voltages. The step change of the voltage sequence is made in the designated ranges of the generator speed, which enables the stabilization of the output voltage in a wide range from the minimum speed of about 25% of the rated speed. Such sequence switching changes the number of pole pairs produced by the winding for each supply sequence. The difference compared to multi-speed induction machines is that, in the presented solution, there is only one winding, not a few, which enables good use of the machine's magnetic core in the same dimensions as for the three-phase machine of a similar power. Steady-state characteristics and dynamic operation were obtained using laboratory measurements of a standalone nine-phase induction generator. The automatic control system maintained the output voltage at the set level, regardless of the generator load and driving power.

Keywords: multiphase cage induction generator; multiphase VSC control; stator supply sequence switching; DC voltage automatic control; wind turbine mechanical characteristics

1. Introduction

A multiphase induction machine (MIM) with number of phases $M > 3$ can operate as a motor or a generator. The idea of MIM operation as a stator converter-controlled multiphase generator [1] was created on the basis of automatic speed control of the multiphase squirrel-cage induction motor presented in [2–4]. The motivation for the use of MIM as an induction generator stemmed from the properties of the machine during motor operation and regenerative braking presented in [2–4]. These were mainly the ability to work with broken stator phases and to work with a constant frequency and voltage at several different characteristic speeds. To achieve this, the supply sequence of the multiphase stator winding must be adapted at each of these speeds. Switching the supply sequence changes the number of pole pairs of the magnetic field. In the ranges between these speeds, MIM control is performed by scalar frequency and voltage control or by vector control. This is the basis for stabilizing the generator voltage when changing its speed over a wide range. The machine has one multiphase winding controlled by a multiphase converter. Details are explained below.

During motor operation, the MIM in Figure 1 is loaded with a mechanical system MECH and directly powered by a PWM-controlled voltage source converter (VSC) during inverter operation, fed from DCSYS.
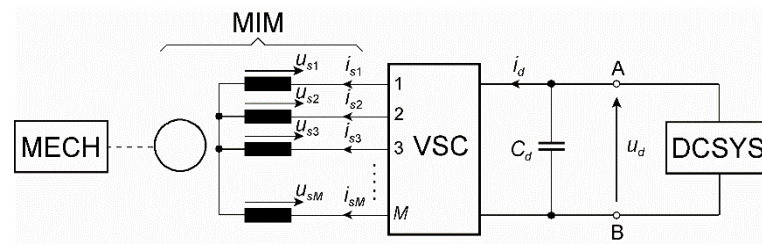
Figure 1. Connection of the *M*-phase MIM with the VSC and the mechanical system MECH.

In order to generate electricity, the drive must be controlled only for generator operation. Then, the MIM is powered from the rotor side by MECH with turbine torque T_E and speed ω_E (e.g., wind or water energy). This allows building an automatic regulation system that stabilizes the voltage between A and B terminals regulating VSC as a PWM rectifier (machine side converter). This time, DCSYS is a loading system, e.g., PWM inverter (grid side converter), operating upon three-phase power system or a resistive load supplied by the auxiliary converter [1,5–9].

Using three-phase or multiphase induction machines as a generator, the minimum speed when the voltage can obtain the nominal (required) value should not be lower than about two-thirds of the nominal speed Ω_N [5,6,10] taken for the rated frequency $f_N = f_0$. For example, from [5,11], it follows that a doubly fed induction generator can work at a speed varying in the range of $(0.7, ..., 1.3)\,\Omega_N$. The method proposed in this paper allows a significant extension of the speed range for a given value of the output voltage, employing the possibility of a stepper change of the phase current sequence. This speed range is from $0.25\,\Omega_N$ to $1.5\,\Omega_N$. For the *M* phase system in Figure 1, the multiphase currents can supply *M* stator windings at $M - 1$ sequences that change the phase shift between adjacent currents as an *m* multiple of $\frac{2\pi}{M}$ [12]. This illustrates the monoharmonic vector of currents,

$$
\begin{bmatrix}
i_{s1} \\
i_{s2} \\
i_{s3} \\
i_{s4} \\
\vdots \\
i_{sk} \\
\vdots \\
i_{sM}
\end{bmatrix}
= I_\mu
\begin{bmatrix}
\cos(\vartheta_s) \\
\cos(\vartheta_s - m\frac{2\pi}{M}) \\
\cos(\vartheta_s - 2m\frac{2\pi}{M}) \\
\cos(\vartheta_s - 3m\frac{2\pi}{M}) \\
\vdots \\
\cos[\vartheta_s - (k-1)m\frac{2\pi}{M}] \\
\vdots \\
\cos[\vartheta_s - (M-1)m\frac{2\pi}{M}]
\end{bmatrix},
\tag{1}
$$

where $\vartheta_s = 2\pi \int_0^t f_s(\tau)d\tau + \vartheta_s(0)$ is the phase angle for the varying angular frequency $\omega_s(t)$, I_μ is the amplitude of all i_{sk} currents, and $m = 0, 1, 2, ..., (M-1)$ is the sequence number. For an $m = 0$ vector, Equation (1) has a so-called zero sequence, where all currents have the same value. For

$$
m = m_{(+)} = 1, 2, ..., m_M,
\tag{2}
$$

we have so-called forward sequences, whereas, for

$$
m = m_{(-)} = M - m_{(+)} = M - 1, M - 2, ..., M - m_M,
\tag{3}
$$

we have so-called backward sequences, opposite to the forward ones, where

$$
m_M = \frac{M - M \bmod 2}{2}.
\tag{4}
$$

For odd sequences, *M* is $m_M = \frac{M-1}{2}$, whereas, for even sequences, *M* is $m_M = \frac{M}{2} - 1$. For example, in a three-phase system, one forward and one backward sequence can be

created apart from the zero sequence. For six phases, $m_M = 2$. Thus, the forward sequences are for $m = m_{(+)} = 1, 2$, backward sequences are for $m = m_{(-)} = 5, 4$, and zero sequences are for $m = 0, 3$.

The mechanical characteristics of a multiphase induction machine indicate the area of work of the multiphase induction generator. Figure 2 shows two typical families of mechanical characteristics of multiphase induction motors using the example of a nine-phase motor from [12]. These families are characteristic of two types of stator windings.
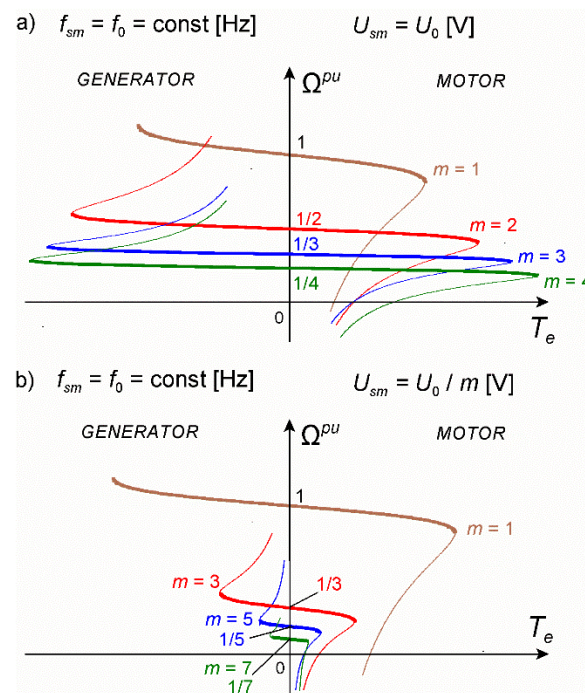

Figure 2. Typical mechanical characteristics of multiphase induction motors at given supply sequences *m*: (**a**) motors with the first type of stator winding; (**b**) motors with the second type of stator winding.

The mechanical characteristics from Figure 2a are typical for MIMs with the winding called here the first type of multiphase winding, whereas the characteristics from Figure 2b are typical for MIMs with the second type of winding. All the characteristics in Figure 2 for a given *m* were determined for the same current frequency $f_{sm} = f_0$ and the RMS phase voltages shown in the figures. For the first type of winding, the voltage is constant $U_{sm} = U_0$, whereas, for the second type of winding, the voltage must be diminished almost proportionally to m ($U_{sm} = \frac{U_0}{m}$), assuring the same level of machine core magnetization. The shape and course of these characteristics for the generator mode show that, at different speeds, only the MIM with the first type of winding enables maintaining the same voltage and frequency by switching the sequence of phase currents. A multiphase machine with the second type of winding can work, in practice, with the sequence $m = 1$.

Both types of multiphase windings have a symmetrical structure, and they differ in the produced MMF harmonic spectrum. The structures of these winding are schematically shown in Figure 3a,b.

For simplicity, these phase windings are represented by single coils. In Figure 3c,d, the MMF distributions F_{ph1} produced by the first phase of these windings are shown. In fact, the single coils are replaced by groups of coils placed in stator slots producing a step-shaped MMF. The first type and the second type of winding are signed with the coefficient $S = 1$ and $S = 2$, respectively.
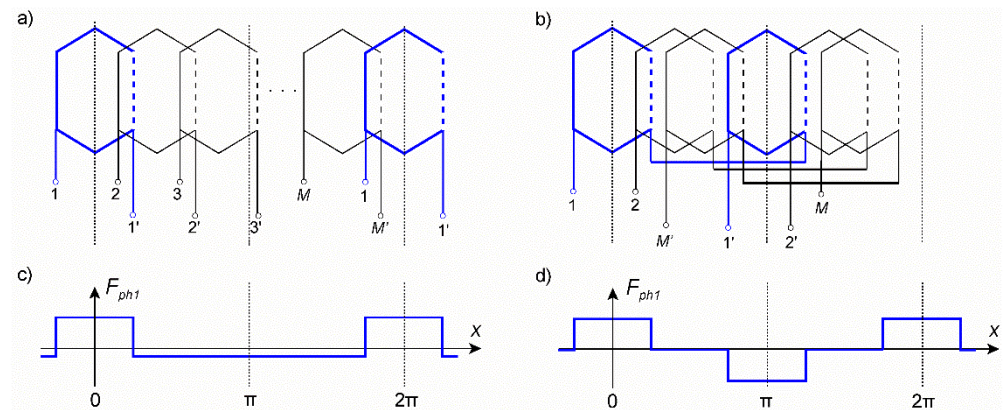
Figure 3. Illustration of two types of multiphase windings composed of single coils: (**a**) structure of the first winding type (*S* = 1) where phases are single coils; (**b**) structure of the second winding type (*S* = 2) composed of single coils; (**c**) F_{ph1}—magnetomotive force (MMF) distribution of the first phase corresponding to the first winding type, (**d**) F_{ph1}—MMF distribution of the first phase corresponding to the second winding type (*x*—machine angle along the air-gap).

The MMF distribution of *k*-th phase winding can be described by the following Fourier series:

$$F_{phk}(x) = \sum_{\nu \in H_\nu} F_k^{(\nu)} = i_{sk} \frac{2}{\pi} N_{sk} \sum_{\nu \in H_\nu} \frac{k_{sk}^{(\nu)}}{\nu} \cos \nu (x - x_k), \tag{5}$$

where $k = 1, 2, 3, ..., M$, i_{sk} is the current of the *k*-th phase winding, ν represents the harmonic orders belonging to the set H_ν, *x* is the machine angle along the air-gap, x_k is the position of the winding magnetic axis, and $k_{sk}^{(\nu)}$ is the winding factor for a given ν. For the 2*p* pole phase windings mutually displaced by the angle $\frac{2\pi}{pM}$, having the same turn numbers $N_{sk} = N_s$ and the same winding factors $k_{sk}^{(\nu)} = k_s^{(\nu)}$ for $\nu = \nu'p$, the MMF distribution can be described as

$$F_{phk}(x) = i_{sk} \frac{2}{\pi p} \sum_{\nu' \in H_\nu'} W_s^{(\nu')} \cos \nu'(x' - x_k'); \ W_s^{(\nu')} = \frac{N_s k_s^{(\nu')}}{\nu'}; \ x_k' = (k - 1) \frac{2\pi}{M}. \tag{6}$$

The MMF of the first type of winding (*S* = 1, Figure 3c) has the harmonic orders ν being odd and even multiples ν' of the number of pole pairs *p*. The MMF of the second type of winding (*S* = 2, Figure 3d) contains only harmonics orders ν being odd multiples ν' of *p*. Thus, the set of harmonic orders takes the form

$$H_{\nu'} = \{S(n - 1) + 1; \ n = 1, 2, 3, ...\}. \tag{7}$$

The MMF of the first type of winding has asymmetry with respect to the *x*-axis, whereas MMF of the second type of winding is symmetrical. Thus, the windings for *S* = 1 can sometimes be called asymmetrical windings, and the windings for *S* = 2 can be called symmetrical.

2. Application Suggestions

A multiphase induction generator can be driven by various engines producing a driving torque T_E causing the rotating speed ω_E. For laboratory purposes, it can be a DC separately excited motor, and, in practical applications, it can be a wind or hydro turbine. An important feature of wind turbines is the high variability of speed caused by the load and wind speed. Water turbines have a lower variation in speed. The generator-type family of MIM mechanical characteristics $\Omega^{pu} = f(T_e^{pu})_{|m=1,2,3,4}$ corresponding to the regenerative operation and the characteristics of the driving DC motor are shown

in Figure 4a. Steady operation points occur at the intersection of the MIM mechanical characteristics for $m = 1, 2, 3, 4$ with the characteristics of the DC motor Ω_{E1}^{pu}, Ω_{E2}^{pu}, Ω_{E3}^{pu}, $\Omega_{E4}^{pu} = f(-T_E{}^{pu})$. These points correspond to the power P_N recognized as nominal for the generator (MIM). At all operating points of the mechanical characteristics, for each value of m, the generator produces almost the same voltage and frequency. For the generator driven by the wind turbine (example), the mechanical characteristics are shown in Figure 4b. The wind turbine family of characteristics $\Omega_E^{pu} = f(-T_E^{pu})_{|V^{pu}}$ is given for various values $V^{pu} = 1; 0.8; 0.6; 0.4$ of the wind velocity [1,7,11,13–17]. The black points indicate the maximum power P_E of the turbine for a given wind velocity.

(a)   (b)
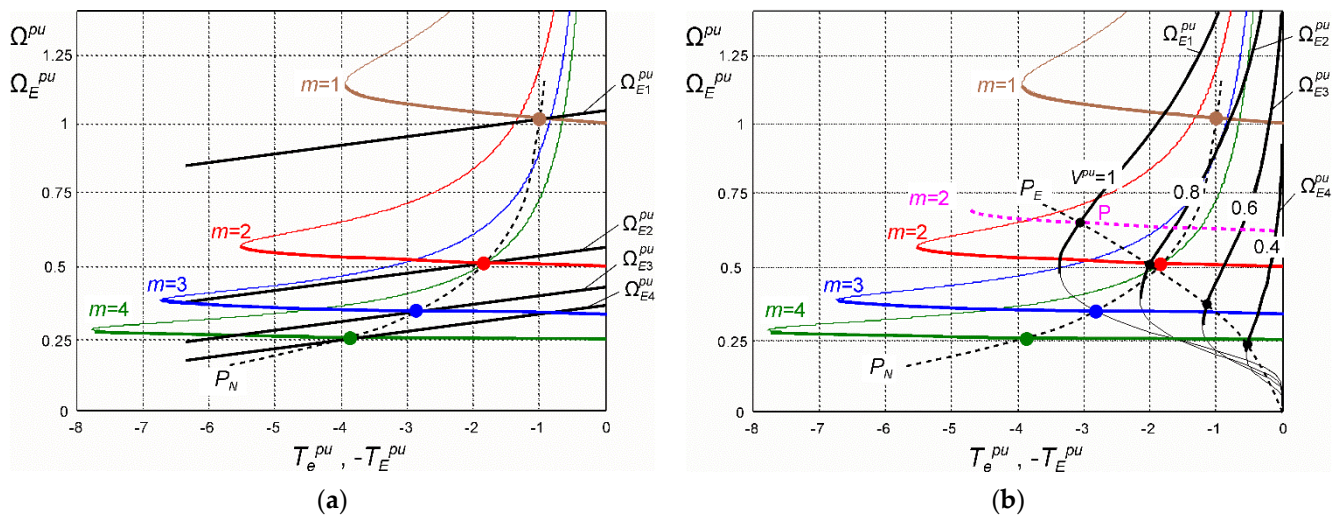
Figure 4. An example of the mechanical characteristics of a multiphase induction generator: (**a**) driven by a DC motor; (**b**) driven by a wind turbine (black thick lines: stable parts of wind turbine mechanical characteristics).

The operation of the generator at points between the MIM characteristics corresponding to given supply sequences m is possible with the frequency and voltage regulation. The largest range of speed occurs between the characteristics for sequences $m = 1$ and $m = 2$. In this range, the appropriate generator speed should be selected, at which point the supply sequence should be switched from $m = 2$ to $m = 1$ with increasing speed or switching from $m = 1$ to $m = 2$ with decreasing speed. Such switching causes a step change in the mechanical characteristics of the generator. For example, when $m = 2$ and speed $\Omega_1^{pu} = 0.51$, the generator works at frequency $f_s^{pu} = m \cdot \Omega_1^{pu} \approx 1$, whereas, at $\Omega_2^{pu} \approx 0.7$, the frequency should be increased to $f_s^{pu} = m \cdot \Omega_2^{pu} \approx 1.4$ at a constant voltage, making the machine overload at point P (magenta curve in Figure 4b). Above this speed, there is a switch to the sequence $m = 1$, and the generator works with the frequency $f_s^{pu} \approx 0.7$. This frequency increases to 1.0 with speed increasing to $\Omega_3^{pu} = 1.0$. The switching of m can practically be performed by introducing a certain hysteresis range. For the speed ranges between the characteristics for the remaining pairs of the supply sequence $m = 2, 3$ and $m = 3, 4$, the switching takes place on a similar principle. To properly set the ranges of operation, some methods can be applied, e.g., maximum power point tracking [7,13,14,16] or appropriate speed choice [5].

For each sequence m, there must be voltage regulation on terminals A–B (Figure 1). A method of field-oriented control of this DC voltage was proposed in [1,7,13], whereas, in [1,6,9,18–20], a standalone generation system together with the grid connection was recognized. According to Figure 1, the VSC between the MIM and the DCSYS is the voltage source inverter. Such a converter system was analyzed among others in [1,5,7,8] for multiphase induction machines. However, three nonconventional solutions for voltage control of variable-speed induction generators were proposed in [16,20,21]. The multiphase

induction and synchronous generators can produce the output voltage at broken phase connections tolerating the machine or converter damages [17,22,23].

The control system proposed in this paper is based on direct regulation of the machine frequency dependent on the electromagnetic torque and the actual speed. The DC voltage is regulated in the output of the PWM rectifier (VSC in Figure 1) and is similar to the method presented in [6]. The proposed method of voltage control is relatively simple as it emphasizes the advantages of voltage control with the use of phase current sequence switching.

Recently, multiphase induction machines were considered as six-phase solutions (applications) [9,17,18,20,24–26] with so called symmetrical and asymmetrical stator windings. The modeling and the control of six-phase generators with a symmetrical stator winding were presented in [17,26], whereas results for those with an asymmetrical stator winding were presented in [9,20,24]. The symmetrical winding has the phases displaced mutually with 60 electrical degrees, while the asymmetrical one has a 30 degree displacement. According to the rules of symmetry, both are symmetrical. Asymmetry can appear, e.g., due to different resistances or inductances of the windings. A better nomenclature is "double stator winding" and the other names proposed in [18].

The MMF of the winding of the first type (Figure 3a,c) has the features of axial asymmetry, while the distribution of the MMF of the winding of the second type is symmetrical in this respect (Figure 3b,d). The properties of the multiphase induction generators, resulting from the magnetic field distribution, are presented in the next sections. They are proven by means of appropriate measurements, for which the guidelines were obtained on the basis of simulations using the computer model presented in [3]. Simulation results were not necessary to be presented in this paper.

3. Properties of MIMs and the Induced Generator Voltage

3.1. MMF Distribution and Main Properties

The influence of both winding types on a multiphase induction machine can be determined by analyzing the traveling total MMF caused by supplying monoharmonic currents (Equation (1)). The total MMF is the sum of phase MMFs for all phase windings.

$$F_s(x) = I_\mu \frac{2}{\pi} \frac{N_s}{p} \sum_{k=1}^{M} \sum_{\nu' \in H_{\nu'}} \frac{k_s^{(\nu')}}{\nu'} \cos\left[\vartheta_s - (k-1)m\frac{2\pi}{M}\right] \cos\nu'\left[px - (k-1)\frac{2\pi}{M}\right]. \quad (8)$$

This expression can be written as a sum of two MMF components,

$$F_s(x) = F_{s1}(x) + F_{s2}(x), \quad (9)$$

where

$$F_{s1}(x) = \frac{1}{2} \sum_{k=1}^{M} \sum_{\nu' \in H_{\nu'}} \frac{2}{\pi p} W_s^{(\nu')} I_\mu \cos[\vartheta_s + (k-1)(\nu'-m)\frac{2\pi}{M} - \nu'px] =$$
$$= \sum_{\substack{\nu' = \nu_1' = (n-1)M + m \in H_{\nu'} \\ n = 1,2,3,...}} F_{(\nu')} \cos(\vartheta_s - \nu'px) \quad , \quad (10)$$

$$F_{s2}(x) = \frac{1}{2} \sum_{k=1}^{M} \sum_{\nu' \in H_{\nu'}} \frac{2}{\pi p} W_s^{(\nu')} I_\mu \cos[\vartheta_s - (k-1)(\nu'+m)\frac{2\pi}{M} + \nu'px] =$$
$$= \sum_{\substack{\nu' = \nu_2' = (n-1)M + M - m \in H_{\nu'} \\ n = 1,2,3,...}} F_{(\nu')} \cos(\vartheta_s + \nu'px) \quad . \quad (11)$$

These MMF components have nonzero values for the harmonic orders ν' marked under the summation sign. The amplitudes of the MMF harmonics for orders ν' have the values

$$F_{(\nu'=\nu'_1,\nu'_2)} = \frac{M}{\pi p} W_s^{(\nu')} I_\mu. \tag{12}$$

Both MMF waveforms $F_{s1}(x)$ and $F_{s2}(x)$ travel with specific rotating speeds. These speeds can be determined for the steady state when $\omega_s = $ constant and $\vartheta_s = \omega_s t$. Equating the arguments of $F_{s1}(x)$ and $F_{s2}(x)$ to zero, we obtain angular speeds $\Omega = \frac{dx}{dt}$ for each harmonic field of $F_{s1}(x)$ and $F_{s2}(x)$, respectively: $\Omega_{\nu'_1} = \frac{\omega_s}{\nu'_1 p}$ and $\Omega_{\nu'_2} = -\frac{\omega_s}{\nu'_2 p}$. Hence, for each ν', the harmonic components of $F_{s1}(x)$ and $F_{s2}(x)$ travel in mutually opposite directions. For each $n = 1, 2, ...,$ the only value that changes the harmonic orders is the sequence number of the supply currents $m = 0, 1, 2, 3, ..., (M - 1)$, where $m = 0$ has to be omitted as not useful. Let us analyze $F_{s1}(x)$ for harmonic orders $\nu'_1 = (n-1)M + m$ and $F_{s2}(x)$ for $\nu'_2 = (n-1)M + M - m$. The greatest and the most important harmonics are for the orders when $n = 1$. Thus, the steady-state MMF monoharmonic waveforms in Equations (13) and (14) for forward sequence numbers in Equation (2) and the winding of the first type $S = 1$ assume the following forms:
for $\nu'_1 = m = m_{(+)} \in H_{\nu'}$

$$F_{s1}(x) = F_{(m_{(+)})} \cos(\omega_s t - m_{(+)} p x), \tag{13}$$

$$F_{(m_{(+)})} = \frac{M}{\pi p} W_s^{(m_{(+)})} I_\mu; \tag{14}$$

for $\nu'_2 = M - m = M - m_{(+)} \in H_{\nu'}$

$$F_{s2}(x) = F_{(M-m_{(+)})} \cos[\omega_s t + (M - m_{(+)}) p x], \tag{15}$$

$$F_{(M-m_{(+)})} = \frac{M}{\pi p} W_s^{(M-m_{(+)})} I_\mu. \tag{16}$$

Waveform $F_{s1}(x)$ rotates with the speed $\Omega_{\nu'_1} = \frac{\omega_s}{mp} = \frac{\omega_s}{m_{(+)} p}$, which is faster than $F_{s2}(x)$ rotating with the speed $\Omega_{\nu'_2} = -\frac{\omega_s}{(M-m)p} = -\frac{\omega_s}{(M-m_{(+)})p}$. For the numbers of backward supply sequence $m = m_{(-)} = M - m_{(+)}$ (Equation (3)), we get the reversed situation for $\nu'_1 = M - m_{(+)} \in H_{\nu'}$, $\nu'_2 = M - M + m_{(+)} = m_{(+)} \in H_{\nu'}$. Now, the speeds assume the following values: $\Omega_{\nu'_1} = \frac{\omega_s}{(M-m_{(+)})p}$, $\Omega_{\nu'_2} = -\frac{\omega_s}{(M-M+m_{(+)})p} = -\frac{\omega_s}{m_{(+)} p}$.

For $S = 2$ (second type of winding) the set of harmonic orders $H_{\nu'} = \{2(n-1) + 1; n = 1, 2, 3, ...\} = \{1, 3, 5, 7, 9, 11, 13, ...\}$ (Equation (7)) having only odd numbers is different than for $S = 1$. This means that, for subsequent sequence numbers $m_{(+)} = 1, 2, ..., m_M$, the harmonic orders must assume values $\nu'_1 = 2(m_{(+)} - 1) + 1$ and $\nu'_2 = 2M - 2(m_{(+)} - 1) - 1$. The angular speeds corresponding to these orders are $\Omega_{\nu'_1} = \frac{\omega_s}{[2(m_{(+)}-1)+1]p}$ and $\Omega_{\nu'_2} = -\frac{\omega_s}{[2M-2(m_{(+)}-1)-1]p}$. For the numbers of backward supply sequence $m = m_{(-)} = M - m_{(+)}$, we get the reversed situation using the same principle as before for $S = 1$.

One of the magnetomotive forces $F_{s1}(x)$ or $F_{s2}(x)$ should be dominant at the sequence number $m = m_{(+)}$ or $m = m_{(-)}$, causing the unambiguous resultant speed of the rotating field. This depends on the amplitudes of $F_{s1}(x)$ and $F_{s2}(x)$ dependent on the ratio $\frac{k_s^{(\nu')}}{\nu'}$. For $\nu'_1 = S(m_{(+)} - 1) + 1$ and $\nu'_2 = SM - S(m_{(+)} - 1) - 1$, the multiphase winding must be designed assuring $\frac{k_s^{(\nu'_1)}}{\nu'_1} > \frac{k_s^{(\nu'_2)}}{\nu'_2}$ [27]. In such a way, the dominant force is $F_{s1}(x)$, whereas $F_{s2}(x)$, playing a parasitic role at this time, rotates oppositely with a lower speed and a lower amplitude. This means that, simultaneously, $F_{s1}(x)$ creates $p_{(+)} = [S(m_{(+)} - 1) + 1]p$ pole

pairs, and $F_{s2}(x)$ creates $p_{(-)} = \left\{SM - [S(m_{(+)} - 1) + 1]\right\}p$ pole pairs. Thus, by setting the sequence number of currents in Equation (1) to the value

$$m = S(m_{(+)} - 1) + 1, \tag{17}$$

for each m_M (Equation (4)), resultant speeds of a positive direction are obtained.

$$\Omega_{0(+)} = \frac{\omega_s}{mp} = \frac{\omega_s}{[S(m_{(+)} - 1) + 1]p}. \tag{18}$$

The respectively opposite speed to Equation (18) appears when $F_{s2}(x)$ dominates. This becomes the case for $m = M - (S(m_{(+)} - 1) + 1)$. Then,

$$\Omega_{0(-)} = -\frac{\omega_s}{(M - m_{(-)})p} = -\frac{\omega_s}{\left\{M - [M - S(m_{(+)} - 1) + 1]\right\}p} = -\frac{\omega_s}{S(m_{(+)} - 1) + 1)p} = -\Omega_{0(+)}. \tag{19}$$

As an example, we have the induction machine with the number of stator phases $M = 7$ and the number of pole pairs $p = 1$. According to Equation (4), the maximum number of forward sequences is $m_M = 3$. The machine with the first type of winding ($S = 1$) has three positive no-load speeds for the supply sequence numbers $m = 1, 2,$ and 3: $\Omega_{0(+)} = \omega_s$, $\Omega_{0(+)} = \frac{\omega_s}{2}$, and $\Omega_{0(+)} = \frac{\omega_s}{3}$. Opposing speeds for this winding type occur for sequence numbers $m = 6, 5,$ and 4: $\Omega_{0(-)} = -\frac{\omega_s}{7-6} = -\omega_s$, $\Omega_{0(-)} = -\frac{\omega_s}{7-5} = -\frac{\omega_s}{2}$, and $\Omega_{0(-)} = -\frac{\omega_s}{7-4} = -\frac{\omega_s}{3}$. For the second winding type $S = 2$ and the same number of phases, we have no-load positive speeds for $m = 1, 3,$ and 5: $\Omega_{0(+)} = \omega_s$, $\Omega_{0(+)} = \frac{\omega_s}{3}$, and $\Omega_{0(+)} = \frac{\omega_s}{5}$, whereas, for $m = 6, 4,$ and 2, we have the corresponding negative speeds: $\Omega_{0(-)} = -\frac{\omega_s}{7-6} = -\omega_s$, $\Omega_{0(-)} = -\frac{\omega_s}{7-4} = -\frac{\omega_s}{3}$, and $\Omega_{0(-)} = -\frac{\omega_s}{7-2} = -\frac{\omega_s}{5}$.

The nine-phase induction machine ($M = 9$, $p = 1$) has the maximum number of forward sequences $m_M = 4$. For the first type of winding $S = 1$, $m = 1, 2, 3,$ and 4, $\Omega_{0(+)} = \omega_s$, $\Omega_{0(+)} = \frac{\omega_s}{2}$, $\Omega_{0(+)} = \frac{\omega_s}{3}$, and $\Omega_{0(+)} = \frac{\omega_s}{4}$. Opposing speeds occur for sequence numbers $m = 8, 7, 6,$ and 5, respectively. For the winding of the second type $S = 2$, $m = 1, 3, 5,$ and 7, $\Omega_{0(+)} = \omega_s$, $\Omega_{0(+)} = \frac{\omega_s}{3}$, $\Omega_{0(+)} = \frac{\omega_s}{5}$, and $\Omega_{0(+)} = \frac{\omega_s}{7}$. The corresponding opposing speeds occur for sequence numbers $m = 8, 6, 4,$ and 2.

To illustrate the above considerations, the distributions of the magnetomotive force generated by the first ($S = 1$) and second type ($S = 2$) of nine-phase windings ($M = 9$) were determined. The schemes of the windings are presented in Figures 5 and 6, respectively, whereas the MMF distributions are shown in Figures 7 and 8 [27].
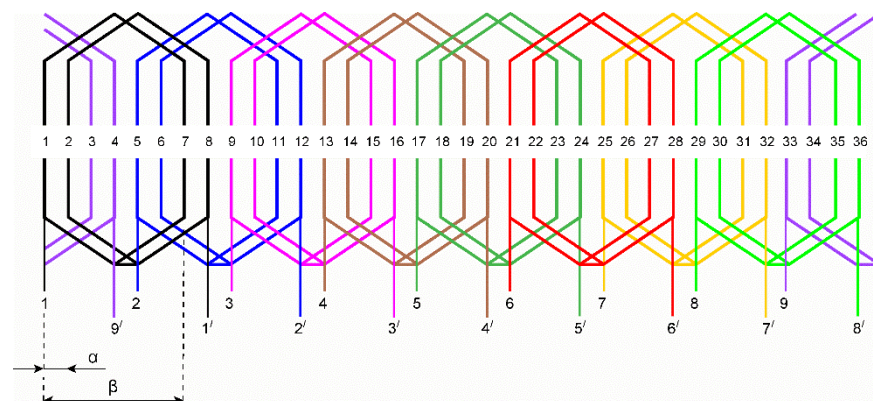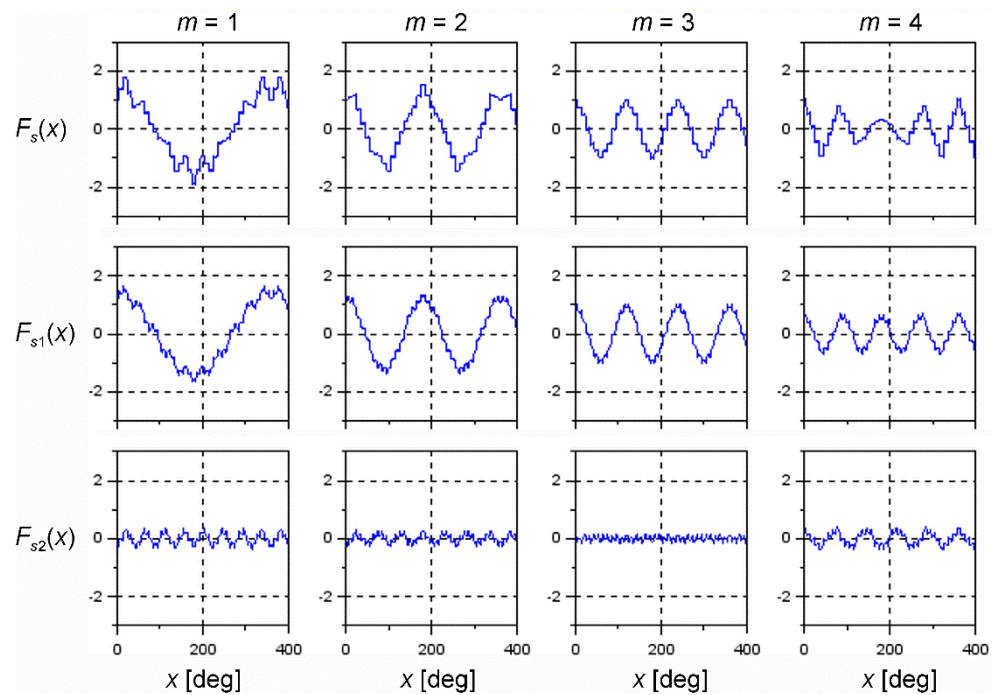

Figure 5. Arrangement of the first type of nine-phase winding ($S = 1$, $M = 9$, $c_g = 2$, $\alpha = 360/Z_s = 360/36 \approx 10°$, $\beta = 6\alpha = 60°$); beginnings of the phase windings: 1, 2, 3 ... ; endings of the phase windings: $1'$, $2'$, $3'$, ...
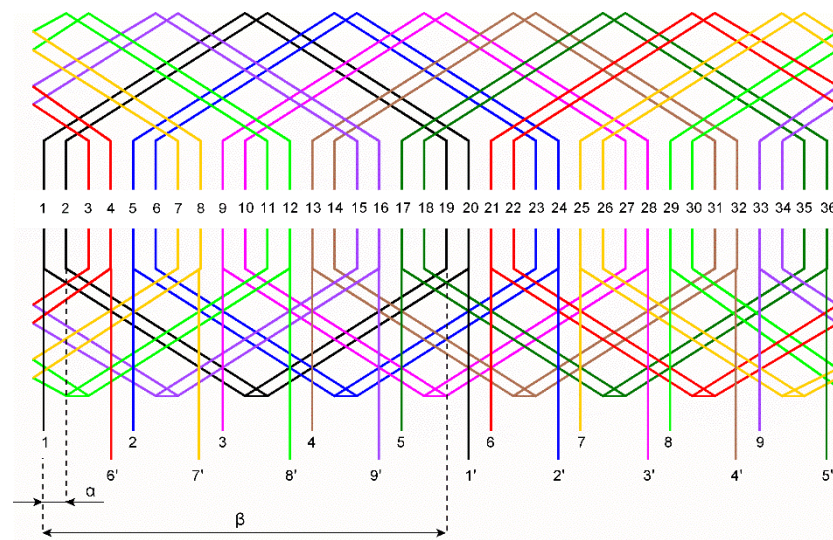
Figure 6. Arrangement of the second type of nine-phase winding ($S = 2$, $M = 9$, $c_g = 2$, $\alpha = 360/Z_s$ = $360/36 \approx 10°$, $\beta = 18\alpha = 180°$); beginnings of the phase windings: 1, 2, 3 . . . ; endings of the phase windings: $1'$, $2'$, $3'$, . . .

Figure 7. Distributions of MMF for nine-phase winding ($M = 9$) of the first type ($S = 1$) at $t = 0$, $I_\mu = 1$, and sequence numbers $m = 1, 2, 3$, and 4.

The angles α and β are indicated in Figures 5 and 6, and c_g is the number of coils in the group creating the phase winding (here, $c_g = 2$). For a typical three phase winding, it is the number of slots per pole per phase, usually denoted as q. For the first type of winding (Figure 5) $S = 1$, $v'_1 = S(m_{(+)} - 1) + 1 = m_{(+)} = m = 1, 2, 3$, and 4, while $v'_2 = SM - S(m_{(+)} - 1) - 1 = 8, 7, 6$, and 5. For the second type winding (Figure 6) $S = 2$, $v'_1 = S(m_{(+)} - 1) + 1 = m = 1, 3, 5$, and 7, while $v'_2 = SM - S(m_{(+)} - 1) - 1 = 17, 15, 13$, and 11. To show that F_{s1} dominates over F_{s2}, the values of ratio $\frac{k_s^{(v'_1)}}{v'_1}$ are presented in Table 1.

They are greater than $\frac{k_s^{(\nu'_2)}}{\nu'_2}$. Additionally, this explains the change in MMF amplitudes seen in Figures 7 and 8.

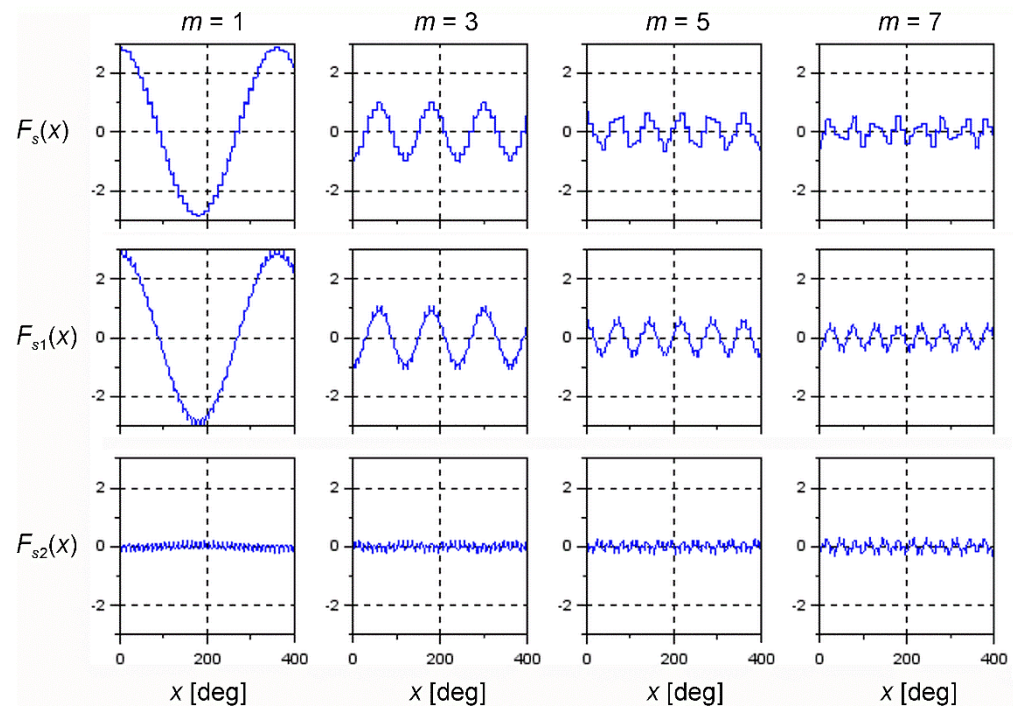**Figure 8.** Distributions of MMF for nine-phase winding ($M = 9$) of the second type ($S = 2$) at $t = 0$, $I_\mu = 1$, and sequence numbers $m = 1, 3, 5$, and 7.

The winding factor for harmonics ν' was calculated according to

$$k_s^{(\nu')} = \sin \nu' \frac{\beta'}{2} \frac{\sin c_g \nu' \frac{\alpha'}{2}}{c_g \sin \nu' \frac{\alpha'}{2}}; \alpha' = p\alpha; \beta' = p\beta. \tag{20}$$

Table 1. Coefficients of the MMF amplitudes and the amplitude of induced phase voltages for the nine-phase windings.

Parameters	First Type Winding (Figure 5) $S = 1$				Second Type Winding (Figure 6) $S = 2$			
$\nu'_1 = m$	1	2	3	4	1	3	5	7
$\nu'_2 = SM - m$	8	7	6	5	17	15	13	11
$k_s^{(\nu'_1)}$	0.4980	0.8528	0.9659	0.8137	0.9961	−0.9659	0.9063	−0.8191
$k_s^{(\nu'_2)}$	−0.6634	−0.4095	0	0.4531	0.0871	−0.2588	0.4226	−0.5735
$\frac{k_s^{(\nu'_1)}}{\nu'_1}$	0.498	0.426	0.322	0.203	0.996	−0.322	0.181	−0.117
$\frac{k_s^{(\nu'_2)}}{\nu'_2}$	−0.083	0.058	0	0.090	0.005	−0.017	0.032	0.052
$\left(\frac{k_s^{(\nu'_1)}}{\nu'_1}\right)^2$	0.248	0.182	0.103	0.041	0.992	0.103	0.033	0.013

This table shows that the dominant component of MMF is F_{s1}, since, for all m, $\frac{k_s^{(\nu'_1)}}{\nu'_1} > \frac{k_s^{(\nu'_2)}}{\nu'_2}$. The values in Table 1 explain the smaller variation of the MMF amplitude for the first type of winding ($S = 1$) than for the winding of the second type ($S = 2$) with a variable supply sequence. For the first winding, the ratios $\frac{k_s^{(\nu'_1)}}{\nu'_1}$ are on a similar level for

m = 1, 2, 3, and 4, whereas, for the second winding, this ratio is several times greater for m = 1 than for the remaining m = 3, 5, and 7. Additionally, the presented $\left(\frac{k_s^{(v_1')}}{v_1'}\right)^2$ values explain why the mechanical characteristics of a multiphase machine with the winding of the first type (Figure 2a) were determined for the same voltage, while the characteristics for the machine with the winding of the second type (Figure 2b) had to be determined for different voltages.

3.2. Induced No-Load Voltage

The resultant magnetomotive force $F_s(x)$ due to the magnetizing current I_μ is described by the relationship in Equation (8) or the form in Equation (9). Thus, the traveling waveform of the flux density in the air-gap,

$$B_\delta(x) = \frac{\mu_0}{\delta} F_s(x),\tag{21}$$

excites the voltages in the machine windings, where δ is the equivalent width of the air-gap, and $\mu_0 = 4\pi \cdot 10^{-7}$ H/m. The voltages are time derivatives of the winding flux linkages. These flux linkages of entire windings should be calculated as the sums of the fluxes linking each of the turns. Instead, these flux linkages can be calculated using substitutional sinusoidal windings. Generally, the winding produces the MMF described by Equations (5) or (6). This means that the MMF determined for a harmonic order $\rho = v'p$ can be produced by series connection of elementary sinusoidal windings of the pole pitch π/ρ and the conductor density.

$$g_k^{(\rho')}(x') = \frac{1}{i_{sk}}\frac{dF_k^{(\rho')}}{dx} = -\frac{2}{\pi}W_s^{(\rho')}\rho'\sin\rho'(x'-x_k'),\tag{22}$$

where $\rho' = \rho/p$, $W_s^{(\rho')} = \frac{N_s k_s^{(\rho')}}{\rho'}$, and $x_k' = (k-1)\frac{2\pi}{M}$.

Flux linkage of the k-th phase winding can be calculated according to the formula developed in [28].

$$\psi_k = \sum_{\rho'\in H_\rho'}\psi_k^{(\rho')} = \sum_{\rho'\in H_\rho'} r_c \int_{-l_c/2}^{l_c/2}\left\{\int_{x_k'-\frac{\pi}{p\rho'}}^{x_k'} g_k^{(\rho')}(x')\left[\sum_{i=1}^{\rho'}\left(\int_{x'+(i-1)\frac{2\pi}{p\rho'}}^{x'+(i-1)\frac{2\pi}{p\rho'}+\frac{\pi}{p\rho'}} B_\delta(x_1')dx_1'\right)\right]dx'\right\}dz,\tag{23}$$

where z is the axial coordinate of the machine, l_c is the length of the stator core, and r_c is the stator core bore radius. The B_δ term is time-dependent. Thus, the time derivative of Equation (23) for the harmonic order ρ' gives the induced steady-state no-load voltage.

$$e_k^{(\rho')} = \frac{d\psi_k^{(\rho')}}{dt} = -E_\mu^{(\rho')}\sin(\omega_s t - \rho'x_k');\; E_\mu^{(\rho')} = \omega_s\frac{2M}{\pi}\frac{\mu_0}{\delta}r_c l_c\left(\frac{N_s k_s^{(\rho')}}{\rho'}\right)^2 I_\mu.\tag{24}$$

The same expression can be obtained from the equivalent circuit of the multiphase induction machine presented in [29]. In Equation (24), the dependence on coordinate z is omitted (e.g., omitted influence of the rotor bar skew). Introducing $\rho' = m$, the amplitude of induced voltage has the following value for $\omega_s = mp\Omega_{0(+)}$ (Equation (18)):

$$E_\mu^{(m)} = mp\Omega_{0(+)}\frac{2M}{\pi}\frac{\mu_0}{\delta}r_c l_c\left(\frac{N_s k_s^{(m)}}{m}\right)^2 I_\mu = \omega_s\Psi_\mu^{(m)},\tag{25}$$

where

$$\Psi_\mu^{(m)} = \frac{2M}{\pi}\frac{\mu_0}{\delta}r_c l_c\left(\frac{N_s k_s^{(m)}}{m}\right)^2 I_\mu.\tag{26}$$

For the speed considered nominal $\Omega_{0(+)} = \Omega_N$ at $m = 1$, the induced voltage is $E_{\mu N}^{(1)} = E_N$. Now, it is apparent that, even if the speed of the generator decreases by a factor of m to $\Omega_{0(+)} = \frac{\Omega_N}{m}$, the voltage amplitude can be increased by switching the supply sequence to m, whereby the voltage then returns to the value E_N as at Ω_N with the same I_μ.

For example, we have the magnetic core of a 4 kW induction machine with a nine-phase winding (Figure 5) placed in 36 stator slots (based on the magnetic core of Sf112M-4). The cage rotor has 28 aluminum bars and the following parameters: $M = 9$, $p = 1$, $\mu_0 = 4\pi \cdot 10^{-7}$ H/m, $r_c = 0.055$ m, $l_c = 0.12$ m, $N_s = 110$, $I_\mu = 2.5$ A, and $\Omega_{max} = 100\pi \approx 314.16$ rad/s for the speed $\Omega_{0(+)} \approx 209.4$ rad/s, not exceeding the maximum one ($f_s = 50/3 \approx 33.34$ Hz, $n_{0(+)} = 2000$ rev/min). The amplitude of the phase voltage (Equation (25)) at $m = 1$ is $E_\mu^{(1)} = 147.6$ V. The flux is $\Psi_\mu^{(1)} = \frac{E_N}{\Omega_N} = 0.7$ Wb, and the RMS voltage is $U_s = E_\mu^{(1)}/\sqrt{2} = 104.3$ V.

Observing values of the coefficient $\left(\frac{k_s^{(v_1')}}{v_1'} \right)^2$ in Table 1, it is clear that only the induction generator with the first type of winding can have its voltage changed by the supply sequence switching. This coefficient appears in Equation (25) for $v_1' = m$ and its value changes from 0.248 for $m = 1$, through 0.182 for $m = 2$ and 0.103 for $m = 3$, to 0.041 for $m = 4$. This means that, to obtain the same voltage at $m = 2$ as at $m = 1$, the magnetizing current has to be increased about 1.36-fold. At $m = 3$, the current has to be increased 2.4-fold. This results from the simplified expression in Equation (25) which takes into account only one harmonic of the magnetic field of the order $v_1' = m$. In fact, such a large increase in the magnetizing current does not occur [25], even at $m = 4$. Equation (25) simply shows the basics of the voltage step change with the parameter m.

Multiphase induction machines with the second type of winding can practically work at the supply sequence number $m = 1$. Such a machine can be designed with almost sinusoidally distributed windings, having all the advantages of fault tolerance of multiphase induction machines [4,17,22,23,25,26].

4. The Control System

As mentioned in Section 1, the control idea is derived from the speed control method presented in [2,4]. Instead of a speed controller, a DC voltage controller is applied. The idea of the control system is presented in Figure 9. It is a kind of development of the system shown in Figure 1.

The induction generator is a multiphase MIM induction machine with a stator winding ST connected to a VSC, while the rotor of a squirrel-cage motor RO is driven by a GE engine at an angular speed ω, directly or by a gear box GB. The output voltage of the capacitance u_d in the DC circuit of the VSC converter is controlled by the CTRL.

The task of the CTRL is to develop impulses controlling the valves of the VSC voltage source converter working as a pulse rectifier for the DC circuit, while the voltage on the capacitance C_d supplies the LOAD. This load can be any two-terminal system or a static converter that produces a standard voltage at the output, e.g., voltages of a three-phase system with a specific amplitude and frequency connected to the power grid (so-called grid converter). Parallel to the capacitance, the circuit UDC0 is connected to maintain the minimum voltage U_{d0} of this capacitor. The controlled output voltage, expressed in relative units u_d^{pu} (in relation to the base reference voltage U^o), should satisfy the dependence $U_{d0}^{pu} < u_d^{pu*}$, where u_d^{pu*} is the desired signal for u_d^{pu}.

The control system CTRL is schematically presented in Figure 10.
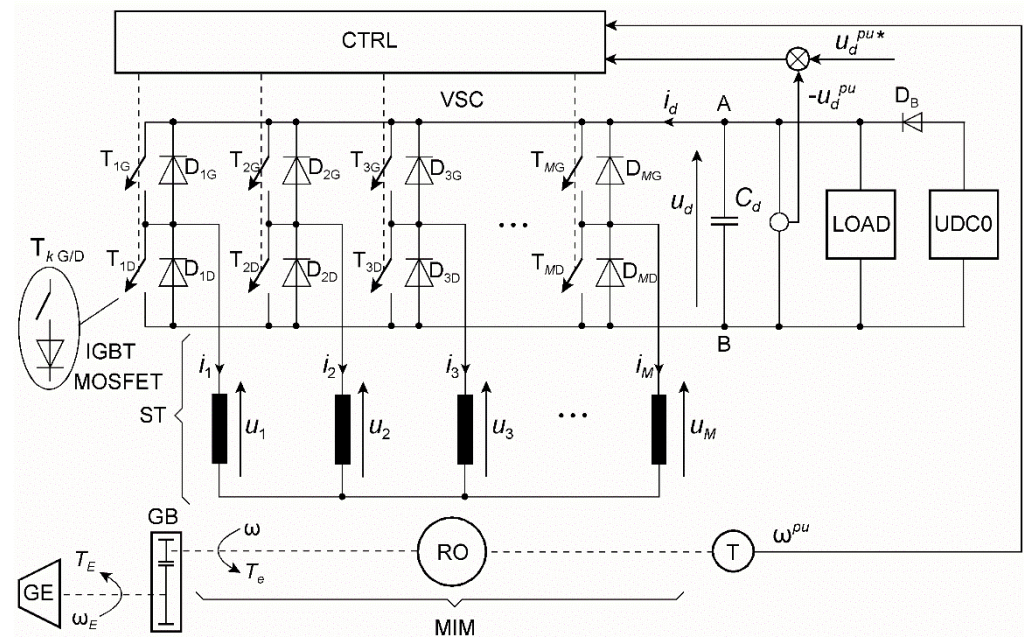
Figure 9. Circuit diagram of a VSC connected with an MIM, operating as a multiphase induction generator: GE—generator engine (e.g., a wind or water turbine), UDC0—system assuring a minimum voltage of C_d, D_B—blocking diode, LOAD—single resistance load (the simplest) power grid supplied with the grid side converter, CTRL—control system, T—speed sensor, GB—gear box (optional), ω^{pu}—relative speed of the MIM machine related to the base reference speed Ω^o.
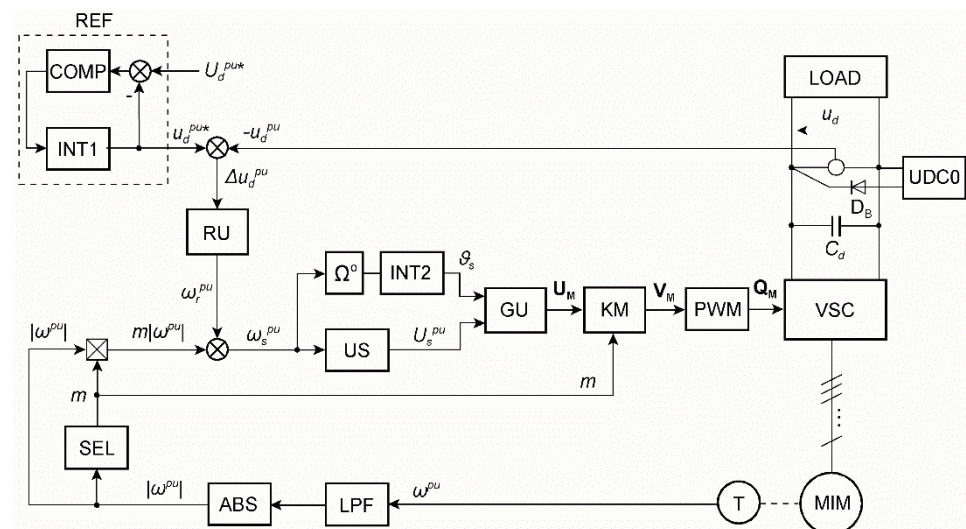
Figure 10. Structure of the control system: REF—voltage reference network shaping u_d^{pu*} as the ramp signal, COMP—comparator, INT1—signal ramp integrator, RU—voltage controller, US—generator of voltage signal U_s^{pu} dependent on ω_s^{pu}, INT2—integrator of stator frequency, GU—generator of M phase control signals, KM—switch of control signals sequence, PWM—pulse width modulator, VSC—voltage source converter, LPF—low-pass filter, ABS—absolute value changer, SEL—selector of supply sequence number m with respect of the MIM speed signal ω^{pu}.

At the base angular frequency $\Omega^o = 2\pi f^o$ ($m = 1$, f^o—base frequency in Hz) the motor speed ω, the stator angular frequency ω_s and the rotor angular frequency ω_r assume the following relative values:

$$\omega^{pu} = p\frac{\omega}{\Omega^o}; \ \omega_s^{pu} = \frac{\omega_s}{\Omega^o}; \ \omega_r^{pu} = \frac{\omega_r}{\Omega^o}. \tag{27}$$

According to Equation (18) the p.u. no-load speed of the machine is $\Omega_0^{pu} = \Omega_0 \frac{p}{\Omega^o} = \frac{\omega_s}{m}$ at $\omega_r^{pu} = 0$. For the machine speed $\omega^{pu} \neq \Omega_0^{pu}$, $\omega_r^{pu} \neq 0$. Thus, for the sequence number m, the stator p.u. frequency is related to the rotor p.u. frequency by the relationship

$$\omega_s^{pu} = m\left|\omega^{pu}\right| + \omega_r^{pu}. \tag{28}$$

The machine slip for a given m is then

$$s^{(m)} = \frac{\omega_s^{pu} - m\omega^{pu}}{\omega_s^{pu}} = 1 - \frac{m\omega}{p\omega_s}. \tag{29}$$

The p.u. amplitude U_s^{pu} is generated by US according to Equation (25), where $U_s^{pu} = \frac{E_\mu^{(m)}}{U^o} = \omega_s^{pu}\Psi_\mu^{(m)pu}$ with the base voltage amplitude $U^o = E_\mu^{(1)} = E_N$ and the base magnetic flux $\Psi^o = \frac{U^o}{\Omega^o}$. Defining the average magnetic flux $\Psi_{\mu AV} = \frac{\Psi_{\mu min} + \Psi_{\mu max}}{2} \approx \Psi_\mu^{(m)}$ for all m and taking into account Equation (28) we have

$$U_s^{pu} = \omega_s^{pu}\Psi_{\mu AV}^{pu} = \left(\left|m\omega^{pu}\right| + \omega_r^{pu}\right)\Psi_{\mu AV}^{pu}. \tag{30}$$

The following values can be used for a nine-phase machine: $\Psi_{\mu min} = \Psi_\mu^{(1)}$, $\Psi_{\mu max} = \Psi_\mu^{(3)}$, or $\Psi_{\mu max} = \Psi_\mu^{(4)}$.

The voltage controller RU can be P type with limited output or PI with saturation. The input signal is the control error $\Delta u_d^{pu} = u_d^{pu*} - u_d^{pu*}$, while the output is the p.u. rotor frequency signal ω_r^{pu} proportional to the electromagnetic torque. The saturation of RU was set to $\omega_{r max}^{pu} = 0.9 s_b^{(1)}$, where $s_b^{(1)}$ is the slip in Equation (29) at which maximum torque occurs when $m = 1$ and $\omega_s^{pu} = 1$.

In the INT2 block, the phase angle is calculated as

$$\vartheta_s = \Omega^o \int_0^t \omega_s^{pu} d\tau. \tag{31}$$

Hence, the block GU generates the vector U_M of M phase monoharmonic signals having the amplitude U_s^{pu} and phase ϑ_s.

$$U_M = \begin{bmatrix} u_1^{pu} \\ u_2^{pu} \\ u_3^{pu} \\ \vdots \\ u_k^{pu} \\ \vdots \\ u_M^{pu} \end{bmatrix} = U_s^{pu} \begin{bmatrix} \sin(\vartheta_s) \\ \sin(\vartheta_s - \frac{2\pi}{M}) \\ \sin(\vartheta_s - 2\frac{2\pi}{M}) \\ \vdots \\ \sin[\vartheta_s - (k-1)\frac{2\pi}{M}] \\ \vdots \\ \sin[\vartheta_s - (M-1)\frac{2\pi}{M}] \end{bmatrix}. \tag{32}$$

The U_M vector signals have the first sequence ($m = 1$).

The sequence of signal in the vector U_M, depending on the parameter m, is changed after passing through the K_M block. This operation takes place according to the following signal conversion:

$$V_M = [v_1^{pu}, v_2^{pu}, v_3^{pu}, ..., v_k^{pu}, ..., v_M^{pu}]^T = K_M U_M. \tag{33}$$

The conversion matrix K_M has a specific form for a given number of phases M, e.g., for $M = 9$,

$$
K_9 = \begin{bmatrix}
1 & & & & & & & & \\
 & k_1 & k_2 & k_3 & k_4 & & & & \\
 & & k_1 & & k_2 & & k_3 & & k_4 \\
 & k_3 & & k_1+k_4 & & & k_2 & & \\
 & & k_3 & k_1 & & & & k_4 & k_2 \\
 & k_2 & k_4 & & & k_1 & k_3 & & \\
 & k_3 & & & k_2 & & k_1+k_4 & & \\
 & k_4 & & k_3 & & k_2 & & k_1 & \\
 & & k_4 & & k_3 & & k_2 & k_1 &
\end{bmatrix}. \tag{34}
$$

In this case, the parameter m can assume the values $m = 1, 2, 3,$ and 4. The coefficients of the K_9 matrix take the value $k_m = 1$ only for a given m, i.e., $k_1 = 1$ for $m = 1$, while $k_2 = k_3 = k_4 = 0$. Similarly, for $m = 2$, there is $k_2 = 1$, while $k_1 = k_3 = k_4 = 0$, etc. The empty cells in the K_9 matrix have the value 0. For a five-phase system ($M = 5$), there is $m = 1, 2$, for a seven-phase system ($M = 7$), there is $m = 1, 2, 3,$ and, for $M = 12$, there is $m = 1, 2, 3, 4, 5$. The relevant K_M matrices are shown below.

$$
K_5 = \begin{bmatrix}
1 & & & & \\
 & k_1 & k_2 & & \\
 & & k_1 & k_2 & \\
 & k_2 & & k_1 & \\
 & & k_2 & k_1 &
\end{bmatrix}, \quad
K_7 = \begin{bmatrix}
1 & & & & & & \\
 & k_1 & k_2 & k_3 & & & \\
 & & k_1 & & k_2 & & k_3 \\
 & & k_3 & k_1 & & & k_2 \\
 & k_2 & & & k_1 & k_3 & \\
 & k_3 & & k_2 & & k_1 & \\
 & & k_3 & k_2 & k_1 &
\end{bmatrix},
$$

$$
K_{12} = \begin{bmatrix}
1 & & & & & & & & & & & \\
 & k_1 & k_2 & k_3 & k_4 & k_5 & & & & & & \\
 & & k_1 & & k_2 & & k_3 & & k_4 & & k_5 & \\
 & k_4 & & k_1+k_5 & & & k_2 & & & k_3 & & \\
 & k_3 & & & k_1+k_4 & & & k_2+k_5 & & & & \\
 & k_5 & & k_3 & & k_1 & & & k_4 & & k_2 & \\
k_2+k_4 & & & & & & k_1+k_3+k_5 & & & & & \\
 & & k_2 & & k_4 & & & k_1 & & k_3 & & k_5 \\
 & k_3 & & & k_2+k_5 & & & & k_1+k_4 & & & \\
 & k_4 & & k_3 & & & k_2 & & & k_1+k_5 & & \\
 & & k_5 & & k_4 & & k_3 & & k_2 & & k_1 & \\
 & & & & & & k_5 & k_4 & & k_3 & k_2 & k_1
\end{bmatrix}.
$$

The PWM block works as the comparator with one carrier triangle signal and the modulating signals in Equation (33). The multiphase system at $M > 5$ seems to be a better and more accurate solution than the PWM modulator. Its operation is based on a comparison of all v_k^{pu} signals with the triangle V_c. For the k-th half-bridge of VSC in Figure 9, the 0–1 output signals of PWM can be described as $q_k = \frac{1+\text{sgn}(v_k - V_c)}{2}$. $q_k = 1$ triggers on the switch T_{kG} and triggers off T_{kD} and vice versa. In this description, the function $\text{sgn}(v_k - V_c)$ can be treated as an ideal comparator. The algebraic signals q_k can be easily changed to logical ones.

The block SEL selects the sequence number m dependent on the actual speed ω^{pu} of the induction generator. Selector work ranges are presented in Table 2. Switching between the sequence numbers must be done by introducing hysteresis margins. The low-pass filter LPF protects SEL against unwanted switching of m.

Table 2. Selection of *m* with respect to speed ranges.

| Speed Range	Sequence Number
$0 < \left\|\omega^{pu}\right\| \leq \frac{1}{m_M}$	$m = m_M$
$\frac{1}{m_M} < \left\|\omega^{pu}\right\| \leq \frac{1}{m_M - 1}$	$m = m_M - 1$
$\vdots$	$\vdots$
$\frac{1}{4} < \left\|\omega^{pu}\right\| \leq \frac{1}{3}$	$m = 3$
$\frac{1}{3} < \left\|\omega^{pu}\right\| \leq \Omega_{12}^{pu}; \Omega_{12}^{pu} = \frac{1}{2}, ..., \frac{2}{3}$	$m = 2$
$\Omega_{12}^{pu} < \left\|\omega^{pu}\right\| \leq 1$	$m = 1$

5. Laboratory Tests of the Nine-Phase Induction Generator

The operation of the nine-phase induction generator ($M = 9$) was tested on a laboratory stand. A machine, previously tested as an electric motor [2,3], was used for this purpose. The machine was built on the magnetic circuit of a 4 kW Sf112M-4 three-phase induction motor, using the first type of stator winding shown in Figure 5 and leaving a squirrel cage rotor with 28 cage bars.

For measurement purposes, the generator power was reduced to P_{dN} = 1000 W at $m = 1$, I_{sN} = 5.3 A (rated RMS stator current), U_{dN} = 150 V (rated mean DC output voltage), f_{sN} = 33.3 Hz (rated frequency), and Ω_N = 209 rad/s (rated speed, maximum speed). The RMS stator phase voltage was $U_{sN} = \frac{\sqrt{2}}{\pi} U_{dN}$ = 67.5 V and the mean DC rated current was $I_{dN} = P_{dN}/U_{dN}$ = 6.67 A. The generator was driven without a gearbox. Thus, $T_E = T_e$ and $\Omega_E = \Omega$. The rated speed was taken as the reference speed $\Omega^o = \Omega_N$, and the rated voltage was the reference voltage $U_d^o = U_{dN}$ for control purposes.

5.1. Measuring System

The scheme of the measuring system is shown in Figure 11, and a photo of the laboratory stand is shown in Figure 12.
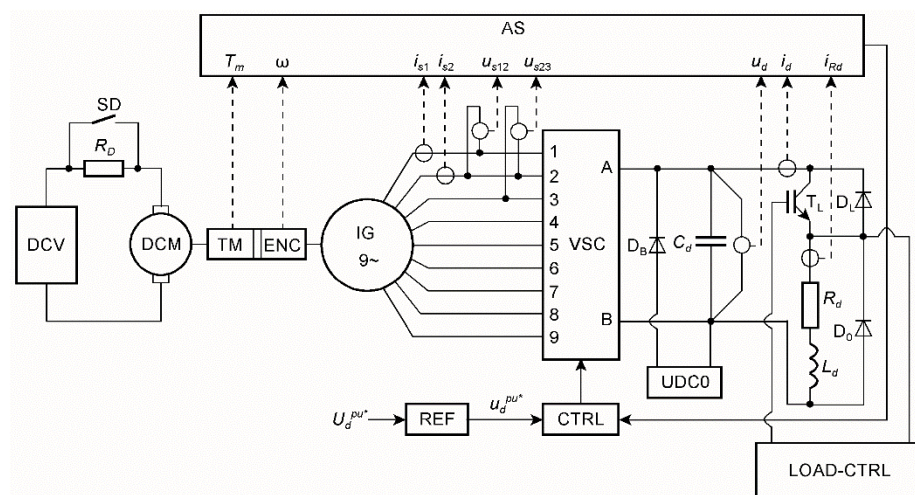
Figure 11. Structure of the test bench: DCV—DC voltage supply, R_D—additional resistance, DCM—DC motor driving the induction generator IG, TM—torque meter, ENC—encoder, N—star point of stator phase windings, AS—acquisition and measurement system, LOAD (T_L, R_d = 8.5 Ω, L_d = 15 mH, D_0), C_d = 4400 μF, DCV—controlled DC voltage supply, R_D—additional resistance shorted by means of SD.
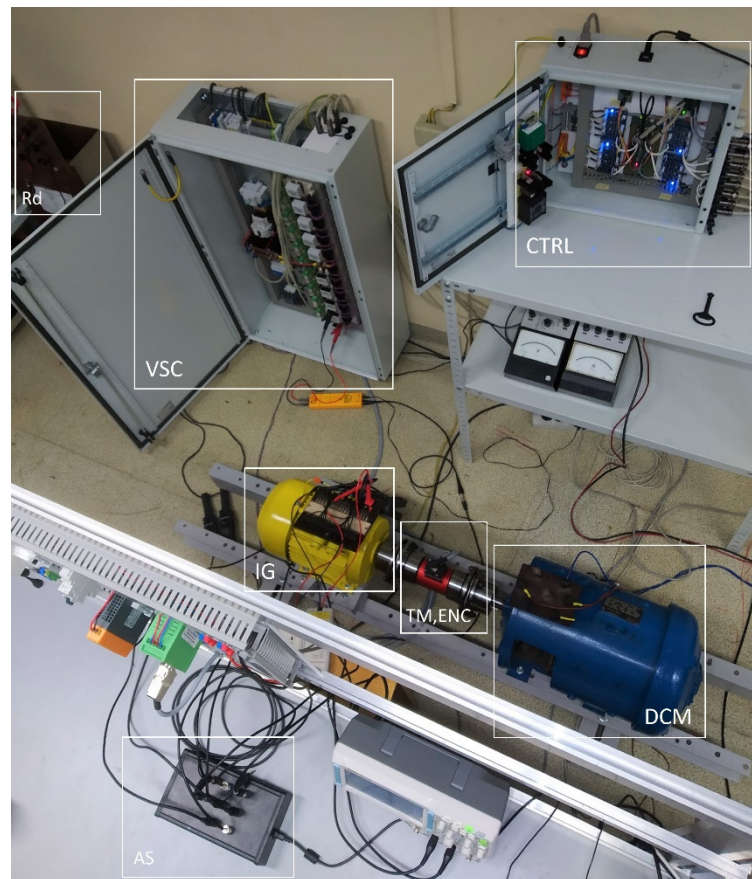
Figure 12. Laboratory test bench view: IG - induction generator, DCM—DC motor, TM—torque meter, ENC—encoder, VSC—IGBT voltage source converter, CTRL—control system, R_d—load resistor, AS—acquisition and measurement equipment.

The main parts of the test bench are listed below.

- Torque meter and encoder (TM, ENC): quadrature encoder 720 imp/rev with the speed sensor built-in DATAFLEX 32/300 torque meter.
- Control system (CTRL) based on digital signal controller: Texas Instruments TMS320F28379D.
- IGBT modules (VSC): Mitsubishi CM50DY-24H.
- Current measurement probes: Chauvin Arnoux E3N; voltage measurement probes: TESTEC TT-SI 9001, PINTEK DP-35.
- Data acquisition card (AS): National Instruments USB-6211.
- DC commutator motor (DCM): 4.5 kW, 220 V, 1460 rev/min.
- UDC0 charges capacitor C_d to initial voltage of U_{d0} = 80 V.

The IG generator was driven by a DC motor. The generator load was the resistance R_d and the inductance L_d, powered by a DC chopper regulated by the width of pulses controlling the T_L transistor. The instantaneous generator output power $p_d = u_d i_d$ supplied the load, while the generator was driven by mechanical power $p_m = T_E \omega$, where $T_e = T_E$. The measured mechanical torque $T_m \approx T_e$. The AS system enabled the measurement of quantities listed on inputs in transient and steady states.

5.2. Experimental Tests

The voltage control system shown in Figure 10 used the simplest method of setting the magnetic flux by proportional adjustment of the phase voltage to the frequency. This provided continuous control combined with step control by switching the winding supply

sequence changing the number of pole pairs. Below are the results of the laboratory tests that demonstrate controllability with some limitations.

5.2.1. Steady-State Measurements

For the steady state, the generator speed was set in the range $\Omega^{pu} = 0.25, ..., 1$. The following values were measured: u_d, i_d, i_{Rd}, ω, T_m, i_{s1}, i_{s2}, u_{s12}, and u_{s23}. A constant value of the output voltage was controlled by an input signal $U_d^{pu*} = 1$. The m switching took place for the following speed ranges (Table 2): $m = 4$ for $0 < \left|\omega^{pu}\right| \leq \frac{1}{4}$, $m = 3$ for $\frac{1}{4} < \left|\omega^{pu}\right| \leq \frac{1}{3}$, $m = 2$ for $\frac{1}{3} < \left|\omega^{pu}\right| \leq \frac{1}{2}$, and $m = 1$ for $\frac{1}{2} < \left|\omega^{pu}\right| \leq 1$. The measured steady-state characteristics are presented in Figure 13.
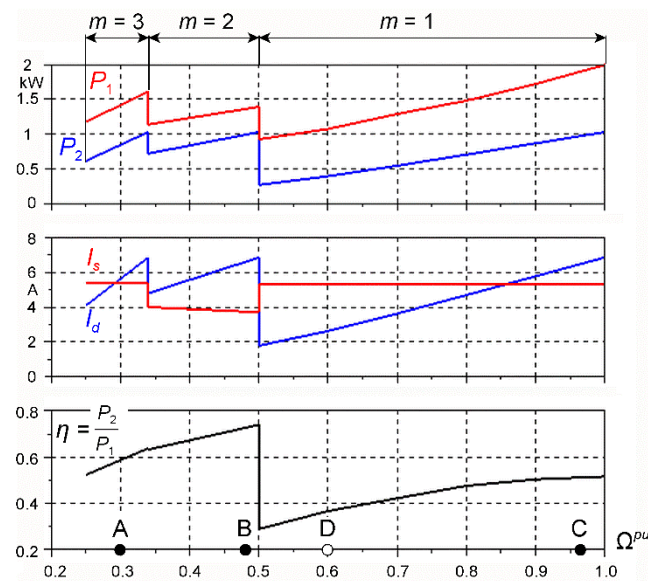
Figure 13. Steady-state characteristics for various values of speed with a constant output voltage $u_d = U_{dN} = 150$ V held by the control system: $P_1 = T_m\Omega$—input power, $P_2 = U_d I_d$—output power, I_s—rms stator current, I_d—mean output current, η—system efficiency, A,B,C,D—distinguished operation cases.

The steady-state characteristics were measured with voltage regulation to a constant value $u_d = U_{dN}$. Depending on the speed range, the sequence number m was switched. The generator load was regulated in such a way that the RMS value of the stator current I_s was kept between $0.75 I_{sN}$ and I_{sN}. This resulted in a load reduction at lower speed. For $m = 4$, the results are not presented because, with the assumed load, it was not possible to generate the desired voltage. With this sequence, the machine produced eight poles, resulting in a high magnetizing current. This current would have to be greater than the rated current at rated output voltage.

In the range of relative speed $\Omega^{pu} = 0.25... 0.5$, the machine worked at $m = 2$ and 3. The best efficiency of $\eta = 0.74$ was obtained with $m = 2$ and $\Omega^{pu} = 0.5$. With $m = 3$ and $\Omega^{pu} = 0.25$, the efficiency dropped to 0.52. Operation in the range marked for $m = 2$ could be partially performed at $m = 3$ and a higher frequency than the rated one, and vice versa.

Operation at $m = 1$ took place in the range $\Omega^{pu} = 0.5... 1$. This interval was the largest for operation with one supply sequence. Although a constant voltage was obtained in the whole range, but at the speed of $\Omega^{pu} = 0.5$, the efficiency of the system decreased dramatically to $\eta = 0.3$. Higher efficiency $\eta = 0.63$ was obtained with $m = 2$ and speed $\Omega^{pu} = 0.6$ (case D in Figure 13), but at the cost of significant current distortion from the sinusoid. Then, the machine worked with the weakening of the magnetic field.

The actual operation of the generator is illustrated in the cases marked A, B, C, and D in Figure 13. The waveforms u_d, i_{Rd}, ω, T_m, i_{s1}, i_{s2}, u_{s12}, and u_{s23} were recorded in the steady state, and the results are shown in Figures 14–17.
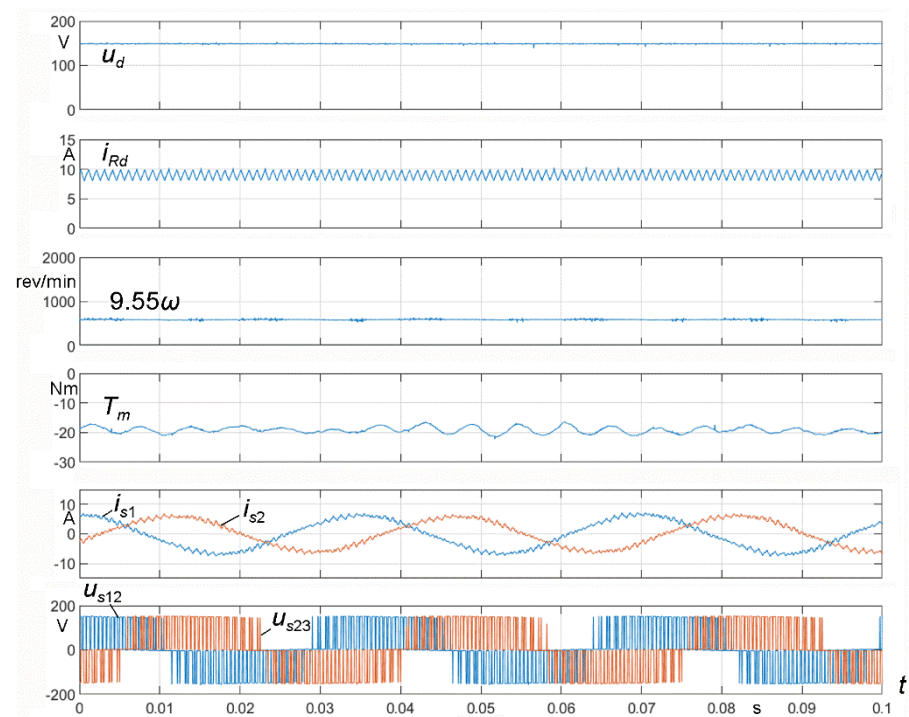
Figure 14. Steady-state waveforms corresponding to case A in Figure 13 at $\Omega^{pu} = 0.3$, $m = 3$.
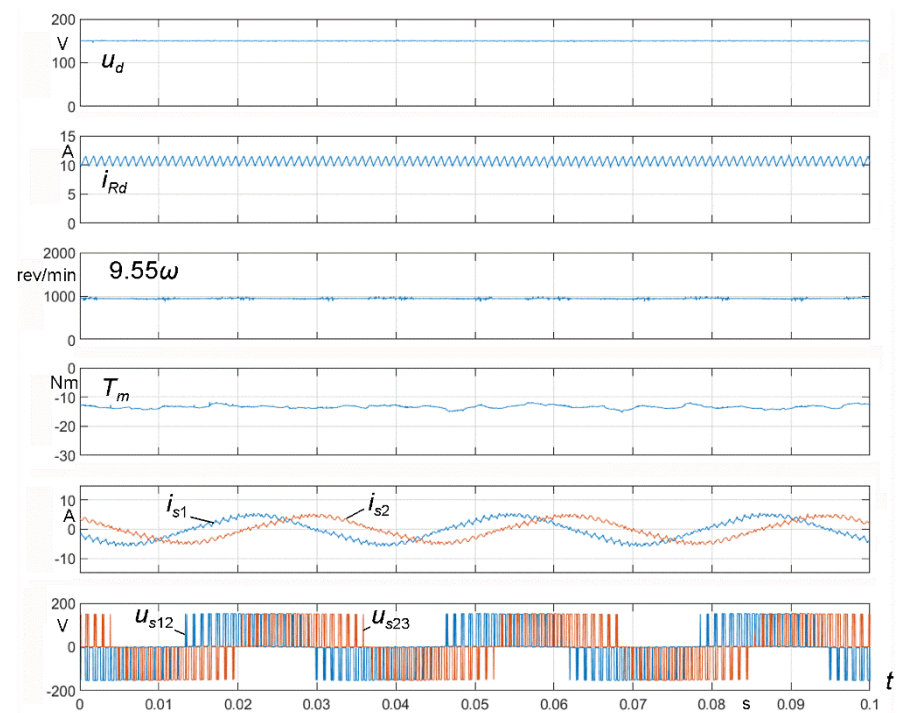

Figure 15. Steady-state waveforms corresponding to case B in Figure 13 at $\Omega^{pu} = 0.48$, $m = 2$.
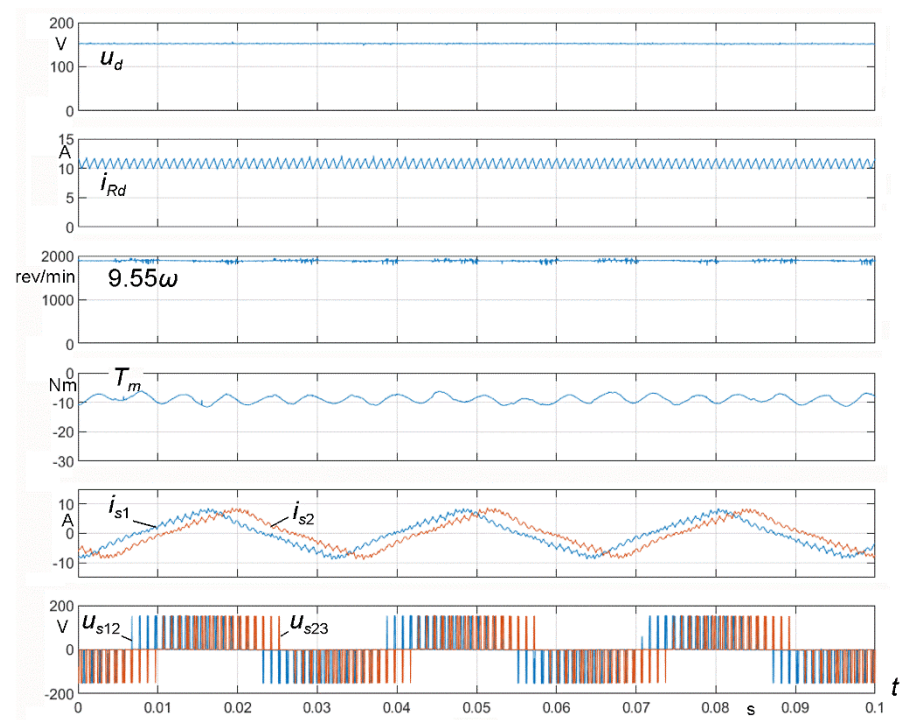
Figure 16. Steady-state waveforms corresponding to case C in Figure 13 at $\Omega^{pu} = 0.96$, $m = 1$.
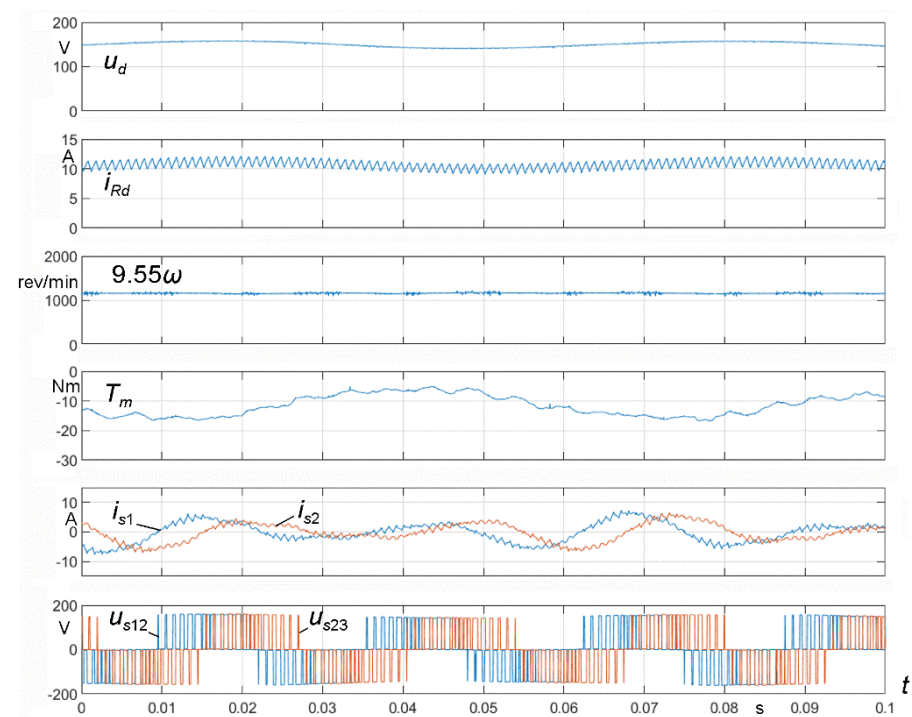

Figure 17. Steady-state waveforms corresponding to case D in Figure 13 at $\Omega^{pu} = 0.6$, $m = 2$.

The work for cases A, B, and C was stable, as the voltage was kept at the set level. The torque T_m showed a slight undulation. For A and B, the phase currents were sinusoidal, but, for C (Figure 16), the currents were triangular. The greatest disturbances in the phase and moment currents, as well as the oscillations of the output voltage and current, occurred in case D (Figure 17). The necessary field weakening in this case was obtained with PWM overmodulation. The advantage, however, is that the desired voltage level was obtained with twice the efficiency of $m = 1$.

5.2.2. Example of Transient States

Figure 18 shows the excitation course of the generator driven at constant speed to the desired voltage $U_{d*} = 150$ V. After excitation, the load was increased to the power $P_d \approx 500$ W. In the 0 s to 5 s time interval, the voltage ramped up linearly from U_{d0} to U_{d*}. The generator was not loaded. The load was increased after 10 s, and the generator was unloaded again after 22 s. All the time, the generator voltage had a constant set value.
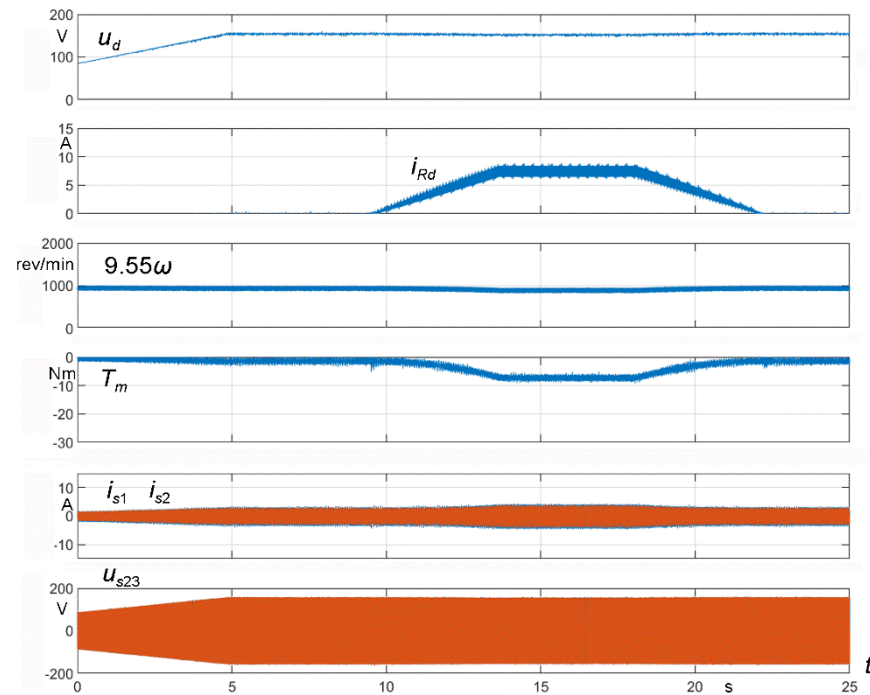

Figure 18. Excitation of the generator at $\Omega^{pu} = 0.48$, $m = 2$ and loading to $P_d \approx 500$ W.

6. Conclusions

From the point of view of voltage regulation, a multiphase induction generator can be driven with any speed, and the voltage can be kept at a desired value. However, when the driving engine does not have a stiff mechanical characteristic, the voltage control must be performed with respect to utilization percentage of the system to produce maximum power. This power can be obtained at a high speed and a low torque, and vice versa. The only problem is the possibility of delivering proper torque resulting from the stable parts of mechanical characteristics of the driving engine (turbine).

The characteristics presented in Figure 13 show that, for the tested generator, the best operation occurred at $m = 2$ and $m = 3$. With $m = 1$, the generator speed range was too large, from $\Omega^{pu} = 0.5$ to $\Omega^{pu} = 1$, in which the voltage had to be regulated to a given value. This range could be divided into operation at $m = 1$ and $m = 2$ assuming a limited speed (Table 2) $\Omega_{12}^{pu} = 2/3$. However, worse operation of the generator at $m = 2$ (Figure 17) should be taken into account.

When considering the generator's drive by means of a wind turbine, it is possible to take into account Figure 4b, where the typical characteristics of the turbine and the characteristics of a multiphase generator were presented. The figure showed that, at different wind speeds, the generator characteristics for $m = 2$ and $m = 3$ were closest to the points of maximum power of the turbine. It follows that the generator should have an optimally designed stator winding with regard to the maximum magnetomotive force at $m = 2, 3$, as well as at $m = 4$. In that case, it would be almost impossible to work with $m = 1$ [27], and the machine would be quite different from the one that was tested. For example, much better properties are obtained using a two-layer winding with the

same pitch as the winding in Figure 5. The design can also use the methodology presented in [30,31].

Advantages of using multiphase induction generators are formulated below.

- A step change in voltage by switching the sequence of phase currents, causing a change in the number of poles of the magnetic field, extends the range of voltage regulation. The most useful is switching between $m = 2$ and 3, between $m = 3$ and 4, etc. Switching between $m = 1$ and 2 at the speed $\Omega^{pu} = 0.5$ causes difficulties in maintaining a sufficiently high efficiency of the generator.
- A multiphase induction generator has only one winding, allowing it to work with a varying number of pole pairs 1, 2, 3, 4, ... When using a Dahlander winding in a three-phase machine, the number of pole pairs can be changed in a ratio of 1 to 2.
- Like a multiphase motor [4,9,17,20,22], the multiphase induction generator tolerates operation with some stator phases broken, allowing the generation of voltage of the desired value.
- The dimensions of a multiphase induction machine are similar to a three-phase machine with the same power. Cage induction machines are cheaper than synchronous generators with permanent magnets, which usually have to work with a back-boost converter.
- Multiphase induction generators can be used in wind and hydropower plants at significantly variable speeds. Even at relatively low speeds, a rated voltage will be produced.
- The best efficiency $\eta = 0.74$ (Figure 13) was not significantly worse than the rated efficiency of the motor Sf112M-4 $\eta_N = 0.88$ (the stator core and the cage rotor were used for the generator), since the generator was working below its rating.

The applied scalar control system maintains the output voltage well at the set level. Similar to motors, better results can be obtained by using spatial vector control or direct voltage regulation and, eventually, sliding mode voltage control [24]. This would be important for smooth switching of the supply sequence number m. When applying a vector control of the output voltage in a wide range of the generator speed, switching of the supply sequence number m must be applied, since the magnetizing current cannot be increased to obtain appropriate flux and voltage because of saturation of the magnetic core.

Author Contributions: Conceptualization, P.D.; methodology, P.D.; software, D.C.; validation, P.D. and D.C.; formal analysis, P.D. and D.C.; investigation, P.D. and D.C.; resources, P.D. and D.C.; data curation, P.D. and D.C.; writing—original draft preparation, P.D.; writing—review and editing, P.D. and D.C.; visualization, P.D. and D.C. All authors have read and agreed to the published version of the manuscript.

Institutional Review Board Statement: Not applicable.

Informed Consent Statement: Not applicable.

Data Availability Statement: Any data presented in the paper may be obtained by contacting the authors.

Conflicts of Interest: The authors declare no conflict of interest.

Glossary

B_δ	flux density in the air-gap
C	capacitance
c_g	number of coils in the group creating the phase winding
E	electromotive force
F	magnetomotive force (MMF)
f_s	stator frequency
$H_\nu, H_{\nu'}$	sets of harmonic orders
i_{sk}	current of k-th phase winding
I_μ	amplitude of stator phase current
l_c	length of the stator core
L	inductance
M	number of phases
m	supply sequence number
m_M	number of sequences for one direction of rotation
N	number of turns
P	power
p	number of pole pairs
R	resistance
r_c	stator core bore radius
S	indicator of machine winding type
T_e, T_E, T_m	torques
U	voltage
V	wind velocity
Z_s	number of stator slots
α	slot angle
β	pitch angle
δ	equivalent width of the machine air-gap
ϑ_s	phase angle
μ_0	vacuum permeability
ν, ν', ρ, ρ'	harmonic orders of MMF Fourier series
ψ	magnetic flux
ω	instantaneous rotational speed
Ω	steady-state rotational speed

References

1. Boldea, I. *Variable Speed Generators (Electric Power Engineering Series)*; CRC, Taylor&Francis Group: Abingdon, UK, 2005; p. 552. ISBN 0849357152.
2. Drozdowski, P.; Cholewa, D. Frequency control of a 9-phase induction motor at switched supply sequence. In Proceedings of the International Symposium on Electrical Machines (SME), Andrychów, Poland, 10–13 June 2018.
3. Cholewa, D.; Drozdowski, P. Simulink modeling of multiphase induction motors. In Proceedings of the 14th Selected Issues of Electrical Engineering and Electronics (WZEE), Szczecin, Poland, 19–21 November 2018.
4. Drozdowski, P.; Cholewa, D. Natural fault tolerance of a nine-phase induction motor drive operating at variable frequency and switched supply sequence. In Proceedings of the 15th Selected Issues of Electrical Engineering and Electronics (WZEE), Zakopane, Poland, 8–10 December 2019.
5. Chen, Z.; Guerrero, J.M.; Blaabjerg, F. A review of the state of the art of power electronics for wind turbines. *IEEE Trans. Power Electron.* **2009**, *24*, 1859–1875. [CrossRef]
6. Kumsuwan, Y.; Srirattanawichaikul, W.; Premrudeepreechacharn, S. A simple voltage and frequency control of VSI-inverter-fed self-excited induction generator drive. In Proceedings of the ICROS-SICE International Joint Conference, Fukuoka, Japan, 18–21 August 2009; pp. 430–434.
7. Jakubowski, B.; Pieńkowski, K. Analysis and synthesis of converter control system of autonomous induction generator with field oriented control. *Arch. Electr. Eng.* **2013**, *62*, 267–279. [CrossRef]
8. Levi, E. Advances in converter control and innovative exploitation of additional degrees of freedom for multiphase machines. *IEEE Trans. Ind. Electron.* **2016**, *63*, 433–448. [CrossRef]
9. Chinmaya, K.A.; Singh, G.K. Modeling and experimental analysis of grid-connected six-phase induction generator for variable speed wind energy conversion system. *Electr. Power Syst. Res.* **2019**, *166*, 151–162. [CrossRef]

10. Baroudi, J.A.; Dinavahi, V.; Knight, A.M. A review of power converter topologies for wind generators. *Renew. Energy* **2007**, *32*, 2369–2385. [CrossRef]
11. Mengjie, L.; Lingxiang, W.; Zhen, X. Control strategy of wide-speed-range doubly fed induction generator, based on stator-winding short circuited in low speed mode. In Proceedings of the 36th Chinese Control Conference (CCC), Dalian, China, 26–28 July 2017. [CrossRef]
12. Drozdowski, P. Speed control of multiphase cage induction motors incorporating supply sequence. *Arch. Electr. Eng.* **2014**, *63*, 511–534. [CrossRef]
13. Thongam, J.S.; Bouchard, P.; Ezzaidi, H.; Ouhrouche, M. Wind speed sensorless maximum power point tracking control of variable speed wind energy conversion systems. In Proceedings of the 2009 IEEE International Electric Machines and Drives Conference, Miami, FL, USA, 3–6 May 2009; pp. 1832–1837. [CrossRef]
14. Ciupageanu, D.A.; Berbece, V.; Tîrșu, M.; Galbura, V. Modeling and control of a low power wind turbine. In Proceedings of the 14th International Conference on Development and Application Systems, Suceava, Romania, 24–26 May 2018. [CrossRef]
15. Ciupageanu, D.-A.; Gheorghe Lazaroiu, G.; Barelli, L. Wind energy integration: Variability analysis and power system impact assessment. *Energy* **2019**, *185*, 1183–1196. [CrossRef]
16. Ramos, T.; Medeiros Junior, M.F.; Pinheiro, R.; Medeiros, A. Slip control of a squirrel cage induction generator driven by an electromagnetic frequency regulator to achieve the maximum power point tracking thales. *Energies* **2019**, *12*, 2100. [CrossRef]
17. Pantea, A.; Yazidi, A.; Betin, F.; Carrière, S.; Sivert, A.; Vacossin, B.; Henao, H.; Capolino, G.-A. Fault-tolerant control of a low-speed six-phase induction generator for wind turbine. *IEEE Trans. Ind. Appl.* **2019**, *55*, 426–436. [CrossRef]
18. Levi, E. Multiphase electric machines for variable-speed applications. *IEEE Tran. Ind. Electron.* **2008**, *55*, 1893–1908. [CrossRef]
19. Duran, M.J.; Barrero, F. Recent advances in the design, modeling, and control of multiphase machines—Part II. *IEEE Trans. Ind. Electron.* **2016**, *63*, 459–468. [CrossRef]
20. Talpone, J.I.; Puleston, P.F.; Cendoya, M.G.; Barrado-Rodrigo, J.A. A dual-stator winding induction generator based wind-turbine controlled via super twisting sliding mode. *Energies* **2019**, *12*, 4478. [CrossRef]
21. Muljadi, E.; Butterfield, C.P.; Handman, D. Dual-speed wind turbine generation. In Proceedings of the National Renewable Energy Laboratory, Prepared for A WEA Windpower '96, Denver, CO, USA, 23–27 June 1996; p. 11.
22. Prieto, I.G.; Duran, M.J.; Garcia-Entrambasaguas, P.; Bermude, M. Field-oriented control of multiphase drives with passive fault tolerance. *IEEE Tran. Ind. Electron.* **2020**, *67*, 7228–7238. [CrossRef]
23. Gonzalez-Prieto, A.; Aciego, J.J.; Gonzalez-Prieto, I.; Duran, M.J. Automatic fault-tolerant control of multiphase induction machines: A game changer. *Electronics* **2020**, *9*, 938. [CrossRef]
24. Amimeur, H.; Aouzellag, D.; Abdessemed, R.; Ghedamsi, K. Sliding mode control of a dual-stator induction generator for wind energy conversion systems. *Int. J. Electr. Power Energy Syst.* **2012**, *42*, 60–70. [CrossRef]
25. Gonzalez-Prieto, A.; Gonzalez-Prieto, I.; Duran, M.J.; Barrero, F. Efficient model predictive control with natural fault-tolerance in asymmetrical six-phase induction machines. *Energies* **2019**, *12*, 3989. [CrossRef]
26. Gonzalez-Prieto, A.; Gonzalez-Prieto, I.; Yepes, A.G.; Duran, M.J.; Doval-Gandoy, J. Symmetrical six-phase induction machines: A solution for multiphase direct control strategies. In Proceedings of the 22nd IEEE International Conference on Industrial Technology (ICIT), Valencia, Spain, 10–21 March 2021; pp. 1362–1367.
27. Drozdowski, P. Synthesis elements of polyphase windings for cage induction motors. *Arch. Electr. Eng.* **1999**, *48*, 63–68.
28. Sobczyk, T.J.; Drozdowski, P. Inductances of electrical machine winding with a nonuniform air-gap. *Arch. Elektrotechnik* **1993**, *76*, 213–218. [CrossRef]
29. Drozdowski, P. Equivalent circuit and performance characteristics of 9-phase cage induction motors. In Proceedings of the International Conference on Electrical Machines ICEM'94, Paris, France, 5–9 September 1994; Volume.1, pp. 118–123.
30. Abdel-Khalik, A.S.; Massoud, A.; Ahmed, S. Standard three-phase stator frames for multiphase machines of prime-phase order: Optimal selection of slot/pole combination. *IEEE Access* **2019**, *7*, 78239–78259. [CrossRef]
31. Abdel-Khalik, A.S.; Massoud, A.M.; Ahmed, S. Nine-phase six-terminal induction machine modelling using vector space decomposition. *IEEE Trans. Ind. Electron.* **2018**, *66*, 988–1000. [CrossRef]